Article:
Vallone, SP, Tantillo, AN, Dos Santos, AM et al. (2019) Giant Barocaloric Effect at the Spin Crossover Transition of a Molecular Crystal. Advanced Materials, 31 (23). 1807334. ISSN: 0935-9648

https://doi.org/10.1002/adma.201807334

Title Giant Barocaloric Effect at the Spin Crossover Transition of a Molecular Crystal

*Steven P. Vallone, Anthony N. Tantillo, Antonio M. dos Santos, Jamie J. Molaison, Rafal Kulmaczewski, Antonin Chapoy, Pezhman Ahmadi, Malcolm A. Halcrow and Karl G. Sandeman**

S. P. Vallone, A. N. Tantillo, Prof. K. G. Sandeman
Department of Physics, Brooklyn College, CUNY, 2900 Bedford Avenue, Brooklyn, NY 11210, USA
Physics Program, The Graduate Center, CUNY, 365 Fifth Avenue, New York, NY 10016, USA
Email: karlsandeman@brooklyn.cuny.edu

Dr. A.M. dos Santos, J.J. Molaison
Neutron Scattering Division, Neutron Sciences Directorate, Oak Ridge National Laboratory, Oak Ridge, Tennessee 37831-6393, USA

Prof. A. Chapoy, Dr. P. Ahmadi
Hydrates, Flow Assurance & Phase Equilibria Research Group, Institute of Petroleum Engineering, Heriot-Watt University, Edinburgh, EH14 4AS, UK

Dr. R. Kulmaczewski, Prof. M.A. Halcrow
School of Chemistry, University of Leeds, Woodhouse Lane, Leeds, LS2 9JT, U.K.

Keywords: spin crossover, barocaloric effect, solid-state cooling, deuteration

We provide the first experimental evidence for a giant, conventional barocaloric effect (BCE) associated with a pressure-driven spin crossover transition near room temperature. We use magnetometry, neutron scattering and calorimetry to explore the pressure dependence of the SCO phase transition in polycrystalline samples of protonated and partially deuterated $[FeL_2][BF_4]_2$ [L = 2,6-di(pyrazol-1-yl)pyridine] in pressures of up to 120 MPa (1200 bar). Our data indicate that, in a pressure change of only 0-300 bar (0-30 MPa), an adiabatic temperature change of 3 K is observed at 262 K or 257 K in the protonated and deuterated materials, respectively. This BCE is equivalent to the magnetocaloric effect (MCE) observed in gadolinium in a magnetic field change of 0-1 Tesla. Our work confirms recent predictions that giant, conventional BCEs will be found in a wide range of SCO compounds.

Caloric cooling is the name given to the use of a "caloric" refrigerant that can be driven between two states of different entropy by means of a field that is conjugate to the order parameter, resulting in an isothermal entropy change, Δs. In the "ferroic" subset of caloric coolants, this results from an intrinsic variation in total entropy in a particular temperature range, associated with a sharply temperature-dependent order parameter.[1] If the field is applied adiabatically, a temperature change, ΔT_{ad} instead results due to an exchange of entropy between degrees of freedom within the refrigerant. Examples of these caloric phenomena include the magnetocaloric effect (MCE), which results from magnetic field-driven changes in magnetization, and the electrocaloric effect (ECE), which occurs when an electric field causes changes in electric polarization. Since caloric refrigerants are typically solids, cooling research is motivated by the opportunity to reduce the global warming effects associated with volatile gas refrigerants as well as by the potential for refrigeration devices to be more efficient. To this end, caloric materials research tends to focus on the size, cyclability and durability of caloric effects at or near room temperature.

Recently, materials which exhibit sizeable mechanocaloric effects – the change of a material's temperature as a result of reversible mechanical deformation – have enjoyed renewed interest. Mechanocaloric effects can be further subdivided into barocaloric effects (BCEs) that involve volume changes caused by a change in the hydrostatic pressure and elastocaloric effects (eCEs) that involve strains brought about by tensile, compressive, or shear stresses. The exploration of mechanocaloric effects is not new; the elastocaloric effect in natural rubber dates to 19th century work by Gough[2] and Joule[3] and there were designs for an elastomer-based refrigerator in the 1990s.[4] Elastocaloric materials research was rekindled by the discovery of giant eCEs in non-magnetic shape memory alloys.[5] Meanwhile, the BCE research field was reignited by the discovery of large BCEs in materials that have giant magnetocaloric effects (GMCEs).[6,7] GMCEs are generally associated with magnetic field-

driven changes in magnetization in the region of first order ferromagnetic or metamagnetic phase transitions which possess large magneto-elastic coupling.[8] Pressure can be used to couple to the change in lattice parameters at such phase transitions.

However, while the magnetocaloric effect and barocaloric effect may be found in the same material, their interdependence is not required *per se*. Optimized BCEs may well be found in materials that have minimal MCEs. Indeed, giant barocaloric effects have recently been observed in a wide range of materials[9] including: Mn_3GaN, a frustrated antiferromagnet around its first order Néel transition;[10] PDMS rubber;[11] and non-magnetic materials where a change in volume is coupled to some other order, such as ferrielectricity[12] or even to polymorphism;[13] On the basis of known thermodynamic parameters, we previously proposed the study of barocaloric effects in spin crossover materials (SCOs) since the volume change at the spin crossover temperature, T_{SCO} is typically large.[14] Recent theoretical modeling has since provided further motivation for experimental work on the barocaloric properties of SCOs.[15,16]

Spin crossover is a spin transition phenomenon that occurs due to the crystal field-induced splitting of *d*-orbitals when an ion such as Fe(II) is placed in a chemical environment. If the resulting energy gap between *d*-orbitals is of the order of the molecular-scale unit of energy (k_BT), electron spins will pair up in those orbitals with the lowest available energy, forming a low spin (LS) state (**Figure 1**) that breaks Hund's first rule of maximizing spin. Above the so-called spin crossover temperature, electrons are excited across the energy gap to the higher energy orbitals, forming a high spin (HS) state that satisfies Hund's rules.[17] This balancing act can be viewed as the interplay between a high spin state favored by entropy and a low spin state favored by enthalpy.[18] The transition between LS and HS states can be continuous or

first order and can exist above room temperature. However, at the lowest temperatures, typically below 100 K, SCO transitions can be kinetically arrested.[19]

Our research concerns a Fe(II) molecular spin crossover compound, $[FeL_2][BF_4]_2$ [L = 2,6-di(pyrazol-1-yl)pyridine], in which Fe(II) ions are connected to 2,6-di(pyrazol-1-yl)pyridine ligands. Two BF_4^- counter anions are present in each formula unit. Polycrystalline samples of the protonated version of this molecule have a low spin, diamagnetic S = 0 ground state, that transitions to a high spin paramagnetic S = 2 state at $T_{1/2,\uparrow}$=262 K on heating (**Figure 2**). The reverse transition is observed at $T_{1/2,\downarrow}$=258 K on cooling and hence the value of T_{SCO} has previously been stated as 260 K.[20] The transition is extremely abrupt, with a width of only 3 K. Rietveld refinement of x-ray diffraction data previously yielded an estimated volume change of 2.6%, which is smaller than some spin crossover compounds but is nonetheless appealing for a study of BCEs when combined with the sharp transition and narrow thermal hysteresis. (The thermal hysteresis associated with spin crossover transition can be tens of Kelvin in some compounds.[17])

To our knowledge, there have been no measurements of the SCO properties of this compound under applied hydrostatic pressure. A Clausius-Clapeyron analysis of the available ambient pressure calorimetric data is therefore instructive. Holland et al. estimated the entropy change at T_{SCO} from differential scanning calorimetry (DSC) measurements, obtaining a value of Δs=66 J mol^{-1}K^{-1}.[20] The magnetic component of this entropy change may be estimated by use of a localized model[21]:

$$\Delta s_{mag} = R\,[\ln(2S_{HS}+1) - \ln(2S_{LS}+1)], \qquad (1)$$

which is thought to be a good approximation for SCO systems,[22] yielding a value of $\Delta s_{mag} = R \ln 3 = 9.13$ J mol^{-1}K^{-1} in the present case. This demonstrates that, in common

with many other SCO systems, the entropy at the spin transition is dominated by lattice effects.[23] The compound has a molecular weight of 651.93 and a volume of around 685 Å^3 / f.u. in the HS state. The relative volume change (2.6%) at the transition therefore equates to $\Delta V \sim 1\times10^{-5}$ m^{3}mol^{-1}. From the Clausius-Clapeyron equation:

$$\Delta s = \Delta V \frac{dp}{dT} \quad , \qquad (2)$$

we may estimate that dT_{SCO}/dp = 152 K/GPa. This large shift of transition temperature with applied pressure is useful for enhancing the ΔT_{ad}[24] and is comparable with other SCO compounds.[14] Its magnitude exceeds the equivalent dT/dp value of several inorganic barocalorics to-date (dT_N/dp = -70 K/GPa in Mn_3GaN,[10] dT_t/dp = +18 K/GPa in a Ni-Mn-In shape memory alloy[6]) and is more comparable with dT/dp values seen recently in organic-inorganic hybrid perovskites (228 K/GPa) that undergo a polymorphic transition.[13] We note that use of the Clausius-Clapeyron relation relies on accurate values of both ΔV and ΔS and so we here have re-measured those quantities using alternative equipment and/or methods as part of our analysis of the barocaloric potential of $[FeL_2][BF_4]_2$.

The effect of pressure on SCO materials has been studied in a few cases previously, and most extensively in $[Fe(phen)_2(NCS)_2]$. We refer the reader to a review by Gütlich et al. for a survey of this literature.[25] We here draw two main points before continuing: first, that the variation of the spin crossover transition temperature with pressure, while monotonic, is not necessarily linear, according to the intramolecular and intermolecular interactions. At the highest pressures, steric hinderance and even pressure-induced, irreversible phase transitions can occur.[26,27] However, for the scope of our work, our emphasis is in demonstrating giant barocaloric effects in the "low pressure", linear region of a pressure, temperature (p,T) phase diagram. Second, while there have been measurements of bulk properties such as

magnetization and high spin fraction of SCO compounds under pressure, there have not, to our knowledge, been measurements of the pressure-induced variation of crystal structure.

We therefore first report structural information obtained under hydrostatic pressure. Both the protonated and partially deuterated samples crystallise in the monoclinic $P2_1$ space group (Ref. [20], **Figure S5** and **Table S2**). The protonated sample was subjected to neutron diffraction in a gas cell at pressures up to 100 MPa. Examples of how the SCO transition can be seen in the raw data are shown in **Figure 3 (right)**. The material is sufficiently crystalline to discern Bragg peaks against the background scattering, and a plot of the refined volume vs temperature on heating yields a $T_{1/2,\uparrow}$~261 K on heating in 20 MPa (Figure 3, left). In applied pressures of 600 bar (60 MPa) the SCO transition is observed at around 265 K (data taken on heating) and in 1000 bar (100 MPa) it is observed at 270 K (data taken on cooling). Since the thermal hysteresis (see later calorimetry data) is still 4 K in this pressure range, the average dT_{SCO}/dp value can calculated as (270-258)/1000 = 120 K/GPa. However, a second, deuterated sample yielded improved diffraction statistics. The 65% deuteration (see Experimental Section) lowered the T_{SCO} by 5 K to 255 K, which is consistent with other deuterated SCO compounds.[28,29] The values of $T_{1/2,\uparrow}$ and $T_{1/2,\downarrow}$ obtained by magnetization (**Figure 2**) are 257 K and 253 K, respectively and so the hysteresis width of the transition is relatively unaffected by deuteration.

The results of Rietveld refinement of diffraction data from the partially deuterated sample under pressures of 400 bar (40 MPa) and 1200 bar (120 MPa) are presented in **Figure 4.** The sparse data are due to the time taken to collect good statistics and are not necessarily indicative of any broadening of the transition. The plot of refined volume vs temperature on heating yields $T_{1/2,\uparrow}$~269 K on heating in 120 MPa, corresponding to dT_{SCO}/dp ~100 K/GPa.

The data concerning the lattice parameters are also shown; we see that the *c*-axis lattice parameter is mainly responsible for the expansion at the phase transition. In addition, there is a change of the crystallographic β-angle across the transition (see Supplementary Information).

While previous studies on SCO compounds have found evidence for pressure-driven criticality,[30] we do not observe any large-scale change in the sharpness of the SCO transition in the low pressures accessed in our neutron diffraction experiments. We can be definitive about this because of magnetometry measurements on the protonated compound taken in 1 Tesla of magnetic field in a clamp cell at pressures up to 4.9 kbar (490 MPa). These are shown in **Figure 5**. The data were taken at applied pressures of 120, 200 and 490 MPa and then a final set of data was taken at ambient pressure. We note three features: first, the SCO transition is sharp up to 200 MPa and only seems to broaden at the highest measured pressure. Second, the change in magnetization at the SCO transition is irreversibly diminished at the highest pressure, 490 MPa, indicating that some portion of the sample has undergone a structural transition to a state that does not host SCO. Such irreversible transitions have been seen in, for example $[Fe(PM\text{-}PEA)_2NCS_2]$ (PM-PEA = *N*-{2-pyridylmethylene}aminobiphenyl).[27] This aspect will be of interest for future studies, but we note that the pressure required to induce an irreversible loss of magnetization greatly exceeds the range of pressure in which we focus our interest in practical BCEs. Third, the variation of T_{SCO} with temperature is not uniform: the initial response is $dT_{SCO}/dp \sim 100$ K/GPa but this dT_{SCO}/dp increases in pressures up to 200 MPa. As shown in Figure 5 (right), the material's response to pressure is much slower (stiffer) at the highest pressures, indicating that there are several regimes of pressure response (indicated as Regions I, II and III in the figure), with steric hindrance possibly becoming evident at the highest pressures. Such S-

shaped (p,T) phase lines have been seen previously, in $[CrI_2(depe)_2]$ (depe = 1,2,-*bis*{diethylphosphino}ethane).[26]

Having mapped out the phase diagram of deuterated $[FeL_2][BF_4]_2$ under pressure, we now turn to the barocaloric effect. Calorimetry data in ambient pressure and 19 and 43 MPa are shown on heating and cooling in **Figure 6**. From measured heat flux, $\dot{Q}$, we calculate $\frac{dQ}{dT} = \frac{\dot{Q}}{\dot{T}}$. We see that in only 19 and 43 MPa, the SCO transition temperature (as given the peak in heat capacity) is increased by around 2 and 5 Kelvin respectively, giving good grounds for finding an irreversible adiabatic temperature change of the same magnitude in each case.

By integrating the heat flow over a temperature range, we can find the entropy with respect to some baseline value, s_0 which is the entropy at some initial temperature, T_0:

$$s(p,T) - s_0(p,T_0) = \int_{T_0}^{T} \frac{1}{T}\left(C_p + \frac{dQ}{dT}\right)dT \,, \qquad (3)$$

as detailed by Stern-Taulats et al., [31] this is an appropriate means of analysis as we are concerned with the change of entropy through the transition instead of specific values of the entropy. From the pressure-dependent volume data at temperatures above and below the phase transition, we may approximate the pressure dependence of the total entropy away from T_{SCO} via a Maxwell relation and therefore estimate $s_0(p,T_0)$ for the 3 pressures studied.[32] The result is a small decrease in the $s_0(p,T_0)$ value as pressure is increased. The temperature, T_0, used for the entropy baseline is 251 K.

From the resulting graph (Figure 6, right) we find a giant caloric change of entropy at the transition of around 86 $J^{-1}kg^{-1}K^{-1}$ (56 J $mol^{-1}K^{-1}$) on heating in ambient pressure. This value is slightly lower than that (66 J $mol^{-1}K^{-1}$) originally measured by Holland et al.[20] While the change of measurement method may account for this slight discrepancy, deuteration is likely

to play a significant role. Previous studies have shown ~10% reduction in the entropy change associated with spin crossover in partially or completely deuterated compounds.[28,34] In the case of Ref. [34], the 10% drop in transition entropy change occurs for a much smaller level of deuteration than in this work.

Pressure, too, has an effect on the observed transition entropy change. **Figure 6** (right) shows the that, from an ambient pressure value of around 86 $J^{-1}kg^{-1}K^{-1}$, the entropy change on heating is slightly reduced to 76 $J^{-1}kg^{-1}K^{-1}$ in 19 MPa and further reduced to 68 $J^{-1}kg^{-1}K^{-1}$ in 43 MPa. We note that the isothermal difference in $s(p,T)$ values above the spin crossover is larger than should be expected from a separate use of the Maxwell relation on that side of the transition; it seems as if the calorimetry signal on heating yields an underestimate of the entropy change through the crossover in applied pressures. We do not find the same experimental feature using the 19 MPa and 43 MPa cooling curves (not shown).

If we assume that the heat capacity away from the phase transition is 3R per mole-atom, which is typical for SCO transition materials in this temperature range,[14] then we may estimate the adiabatic temperature change in 19 MPa and 43 MPa, as shown in Figure 6 (right). If we use the heating curves only, we see that 19 MPa pressure gives rise to a peak, irreversible adiabatic temperature change of 2 K at 257 K, meaning that $d(\Delta T_{ad})/dp$ ~100 K/GPa (10 K/kbar). Similarly, 43 MPa of pressure yields a peak ΔT_{ad} of around 4.5 Kelvin. To put these results in perspective, a temperature change of 2 K is of the same order as a 0-0.7 Tesla magnetic field change acting on Gd at room temperature. Alternatively, the 0-1 Tesla MCE in Gd (ΔT_{ad}~3 K) would equate to a pressure of change of 0-300 bar (0-30 MPa) here. We also note that, in order to fully counteract the 4 K transition hysteresis, a pressure of around 400 bar (40 MPa) is needed. This can be seen in Figure 6 (left): the cooling curve at 43 MPa almost exactly overlaps with the heating curve at ambient pressure.

For this reason, we may directly estimate the maximum reversible ΔT_{ad}.[32] It will be zero for 0-43 MPa and, from the variation of T_{SCO} with pressure in the "low" pressure region I of Figure 4 (right), the peak value of ΔT_{ad} will increase by 1 K per 10 MPa in excess of 43 MPa (e.g. ΔT_{ad} ~ 6 K in 0-100 MPa).

In summary, we have demonstrated the presence of a giant barocaloric effect in a deuterated spin crossover compound near room temperature. Our studies open the way to further study of the detailed nature of the (p,T) phase diagram in other SCOs and, in particular, the nature of the structural response in different régimes of pressure. We note that there are ample ways in which SCO responses can be tuned by ligand, counter anion, and solvate choices and that other compounds may yield even larger dT_{SCO}/dp values and associated barocaloric effects at and above room temperature.

Experimental Section

Sample preparation: The details of preparation of the protonated sample are given elsewhere.[20]

Synthesis of the partially deuterated sample: 2,6-Di(pyrazol-1-yl)pyridine (2 g, 9.5 mmol) was incubated in D_2O (300 cm^3) at 230 °C for 20 hrs, in a Parr autoclave reactor.[35] After cooling to room temperature the aqueous solution was extracted with dichloromethane (3x 50 cm^3), and the dried organic fractions evaporated to dryness to give the deuterated ligand. Yield 1.3 g, 62 %, with an overall deuteration level of *ca* 65 % by mass spectrometry. The product contains a range of partially deuterated $C_{11}D_xH_{9-x}N_5$ molecules with $2 \leq x \leq 9$. Different reactions gave slightly different isotopic distributions, but with the d^6 formulation (x = 6) being consistently the most abundant. ^{13}C NMR spectra demonstrated the deuteration occurs predominantly at the pyrazolyl rings, with the pyridyl C–H groups being relatively

unaffected. Further details are provided in the Supporting Information. The deuterated complex was prepared by reacting $Fe[BF_4]_2 \cdot 6H_2O$ with 2 equiv of the deuterated ligand by the published method.[20]

Neutron scattering under hydrostatic pressure: Data were collected on the Spallation Neutrons And Pressure (SNAP) beamline at ORNL using an aluminum pressure cell (with weak attenuation). Data on the protonated compound were taken in continuous mode, i.e. faster acquisition in controlled, continuous heating or cooling at 20 MPa (200 bar, heating), 60 MPa (600 bar, heating), and 100 MPa (1000 bar, cooling). Data on the deuterated compound were taken in continuous mode, upon heating at ambient pressure and 40 MPa (400 bar) and upon heating and cooling at 120 MPa (1200 bar).

Magnetometry: Magnetisation vs. temperature data were taken in a Quantum Design SQUID magnetometer. Pressure was applied via a custom-made clamp cell made from a non-magnetic CuBe alloy. The sample was placed in a Teflon capsule (Ø=2.5 mm, h=10 mm) along with fluorinert as pressure medium and a small piece lead as a pressure manometer. The pressure on sample was determined by tracking the pressure dependent superconducting transition of lead[36] up to 490 MPa. A fixed field of 1 Tesla was applied for all measurements.

Differential scanning calorimetry under hydrostatic pressure: Data were collected using a Calvet calorimeter (SETARAM BT2.15 model). The calorimeter is a differential scanning calorimeter equipped with one measurement cell and one reference cell both rated up to 60 MPa. The temperature of the calorimeter is controlled using liquid nitrogen and internal heaters for cooling and heating purposes, respectively. The measurement cell and reference cell are surrounded by 3D Calvet sensors for precise measurement of heat flow. Measurements were carried out at three distinct pressure values: ambient pressure; and applied pressures of 19 and 44 MPa. Temperature T and heat flow $\frac{dQ}{dt}$ were measured every

10 seconds, leading to discernable temperature steps dT equal to the difference between successive temperature readings. The differential heat input can be found by $dQ = dt \times \frac{dQ}{dt}$. We can then find the constant pressure heat capacity by applying the equation $C_p = \frac{1}{m}\frac{dQ}{dT}$, where m is the mass of the sample in the calorimeter. Entropy change estimates were obtained by trapezoidal integration.

Supporting Information
Supporting Information is available from the Wiley Online Library or from the author.

Acknowledgements
We are grateful to L. Mañosa for useful discussions. S.P.V., A.N.T. and K.G.S acknowledge that support for this project was provided by a PSC-CUNY Award, jointly funded by The Professional Staff Congress and The City University of New York. R. K. and M. A. H. thank Prof. John Blacker and Dr. Will Reynolds (Institute of Process Research and Development, University of Leeds) for access to the autoclave reactor, and the EPSRC for funding (EP/K012568/1). A portion of this research used resources at the Spallation Neutron Source, and the Center for Nanophase Materials Science, both DOE Office of Science User Facilities operated by the Oak Ridge National Laboratory.

Received: ((will be filled in by the editorial staff))
Revised: ((will be filled in by the editorial staff))
Published online: ((will be filled in by the editorial staff))

References

[1] I. Takeuchi, and K. Sandeman, *Phys. Today*, 2015, *68*, (12), 48–54.

[2] J. Gough, *Mem. Lit. Philos. Soc. Manchester*, 1805, *1*, 288–295.

[3] J.P. Joule, *Philos. Trans. R. Soc. London*, 1859, *149*, 91–131.

[4] A. DeGregoria, United States Patent 5,465,781. issued 1995.

[5] L. Mañosa, D. González-Alonso, A. Planes, E. Bonnot, M. Barrio, J.-L. Tamarit, S. Aksoy, and M. Acet, *Nat. Mater.*, 2010, *9*, (6), 478–81.

[6] L. Manosa, D. Gonzalez-Alonso, A. Planes, E. Bonnot, M. Barrio, J.-L. Tamarit, S. Aksoy, and M. Acet, *Nat. Mater.*, 2010, *9*, (6), 478–481.

[7] L. Mañosa, D. González-Alonso, A. Planes, M. Barrio, J.-L. Tamarit, I.S. Titov, M. Acet, A. Bhattacharyya, and S. Majumdar, *Nat. Commun.*, 2011, *2*, 595.

[8] V. Pecharsky, K. Gschneidner, A. Pecharsky, and A. Tishin, *Phys. Rev. B*, 2001, *64*, (14), 144406.

[9] L. Mañosa, and A. Planes, *Adv. Mater.*, 2017, *29*, (11), 1603607.

[10] D. Matsunami, A. Fujita, K. Takenaka, and M. Kano, *Nat. Mater.*, 2015, *14*, (1), 73–78.

[11] A.M.G. Carvalho, W. Imamura, E.O. Usuda, and N.M. Bom, *Eur. Polym. J.*, 2018, *99*, 212–221.

[12] P. Lloveras, E. Stern-Taulats, M. Barrio, J.-L. Tamarit, S. Crossley, W. Li, V. Pomjakushin, A. Planes, L. Mañosa, N.D. Mathur, and X. Moya, *Nat. Commun.*, 2015, *6*, (1), 8801.

[13] J.M. Bermúdez-García, M. Sánchez-Andújar, S. Castro-García, J. López-Beceiro, R. Artiaga, and M.A. Señarís-Rodríguez, *Nat. Commun.*, 2017, *8*, 15715.

[14] K.G. Sandeman, *APL Mater.*, 2016, *4*, (11), 111102.

[15] P.J. von Ranke, *Appl. Phys. Lett.*, 2017, *110*, (18), 181909.

[16] P.J. von Ranke, B.P. Alho, and P.O. Ribeiro, *J. Alloys Compd.*, 2018, *749*, 556–560.

[17] P. Gütlich, Y. Garcia, and H. a. Goodwin, *Chem. Soc. Rev.*, 2000, *29*, (6), 419–427.

[18] C. Benelli, and D. Gatteschi, Introduction, in *Introduction to Molecular Magnetism: From TransitionMetals to Lanthanides*, Wiley-Blackwell, pp. 1–23.

[19] N. Paradis, G. Chastanet, and J.-F. Létard, *Eur. J. Inorg. Chem.*, 2012, *2012*, (22), 3618–3624.

[20] J.M. Holland, C.A. Kilner, M. Thornton-Pett, M.A. Halcrow, J.A. McAllister, and Z. Lu, *Chem. Commun.*, 2001, (6), 577–578.

[21] C. Kittel, *Introduction to solid state physics*, Wiley, New York.

[22] M. Sorai, and S. Seki, *J. Phys. Chem. Solids*, 1974, *35*, (4), 555–570.

[23] P. Gütlich, A. Hauser, and H. Spiering, *Angew. Chemie Int. Ed. English*, 1994, *33*, (20), 2024–2054.

[24] K.G. Sandeman, *Scr. Mater.*, 2012, *67*, (6), 566–571.

[25] P. Gütlich, V. Ksenofontov, and A. Gaspar, *Coord. Chem. Rev.*, 2005, *249*, (17–18), 1811–1829.

[26] V. Ksenofontov, A.B. Gaspar, G. Levchenko, B. Fitzsimmons, and P. Gütlich, *J. Phys. Chem. B*, 2004, *108*, (23), 7723–7727.

[27] V. Ksenofontov, G. Levchenko, H. Spiering, P. Gutlich, J.F. Letard, Y. Bouhedja, and O. Kahn, *Chem. Phys. Lett.*, 1998, *294*, (6), 545–553.

[28] K. Hosoya, T. Kitazawa, M. Takahashi, M. Takeda, J.-F. Meunier, G. Molnár, and A. Bousseksou, *Phys. Chem. Chem. Phys.*, 2003, *5*, (8), 1682–1688.

[29] T. Kosone, C. Kachi-Terajima, C. Kanadani, T. Saito, and T. Kitazawa, *Chem. Lett.*, 2008, *37*, (7), 754–755.

[30] P. Gütlich, Y. Garcia, and H. a. Goodwin, *Chem. Soc. Rev.*, 2000, *29*, (6), 419–427.

[31] E. Stern-Taulats, A. Gràcia-Condal, A. Planes, P. Lloveras, M. Barrio, J.-L. Tamarit, S. Pramanick, S. Majumdar, and L. Mañosa, *Appl. Phys. Lett.*, 2015, *107*, (15), 152409.

[32] A. Aznar, P. Lloveras, M. Romanini, M. Barrio, J.-L. Tamarit, C. Cazorla, D. Errandonea, N.D. Mathur, A. Planes, X. Moya, and L. Mañosa, *Nat. Commun.*, 2017, *8*, (1), 1851.

[33] L.M. Moreno-Ramírez, V. Franco, A. Conde, H. Neves Bez, Y. Mudryk, and V.K. Pecharsky, *J. Magn. Magn. Mater.*, 2018, *457*, 64–69.

[34] B. Weber, W. Bauer, T. Pfaffeneder, M.M. Dîrtu, A.D. Naik, A. Rotaru, and Y. Garcia,

Eur. J. Inorg. Chem., 2011, *2011*, (21), 3193–3206.

[35] B. Hachuła, H.T. Flakus, A. Tyl, and A. Polasz, *Chem. Phys. Lett.*, 2014, *599*, 68–72.

[36] M. Garfinkel, and D.E. Mapother, *Phys. Rev.*, 1961, *122*, (2), 459–468.

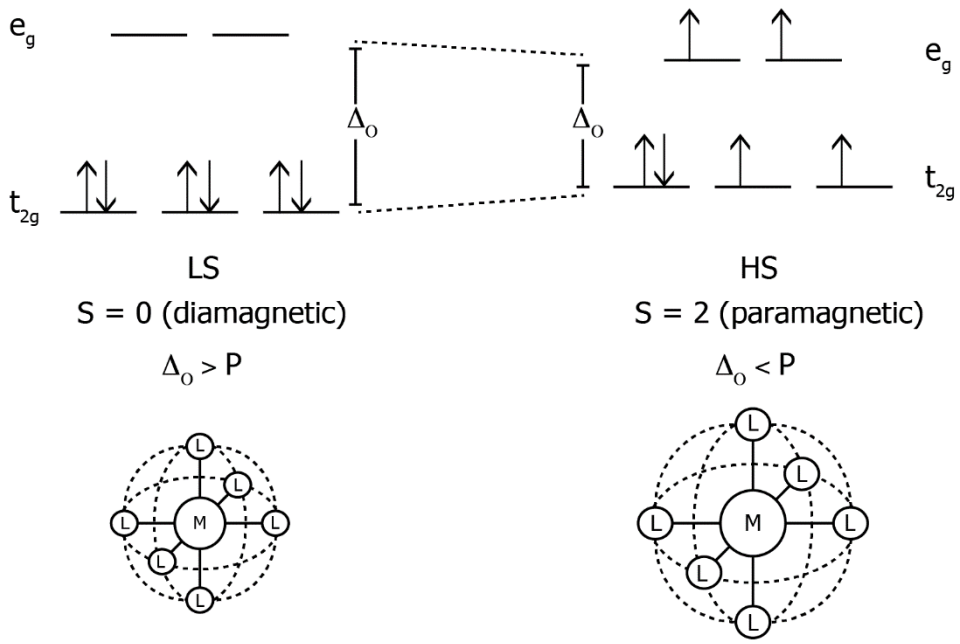

Figure 1. Schematic energy level diagram for an octahedrally-coordinated Fe(II) ion, showing the effect of a crystal field in generating the possibility of a low spin (LS) or high spin (HS) state, depending on the size of the crystal field due to the ligand.

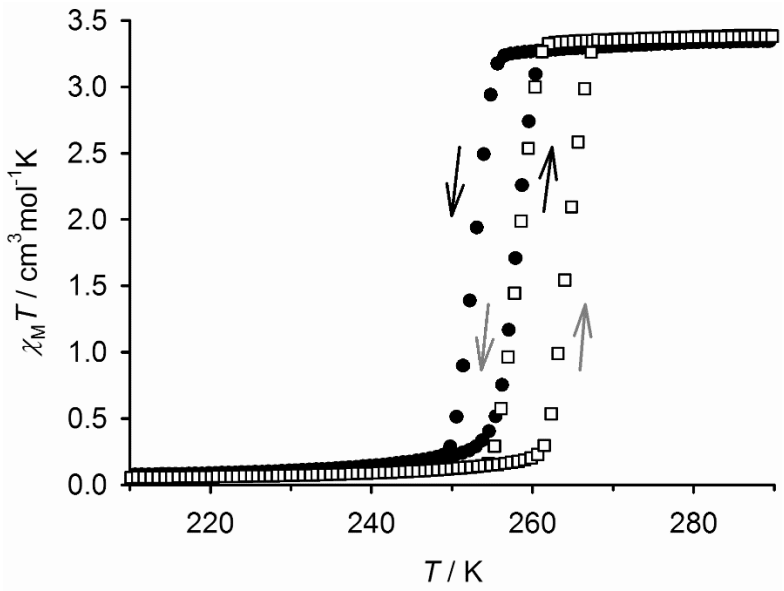

Figure 2. Magnetic susceptibility data for $[FeL_2][BF_4]_2$ in its protio (□) and partially deuterated (●) forms. Both samples were measured at a scan rate of 5 $Kmin^{-1}$. The spin crossover temperatures are in agreement with calorimetry values: $T_{1/2,\uparrow}$ and $T_{1/2,\downarrow}$ are 262 and 258 K in the protio sample and 257 K and 253 K in the partially deuterated sample, respectively. The hysteresis width of the transition is therefore 4 K for both samples.

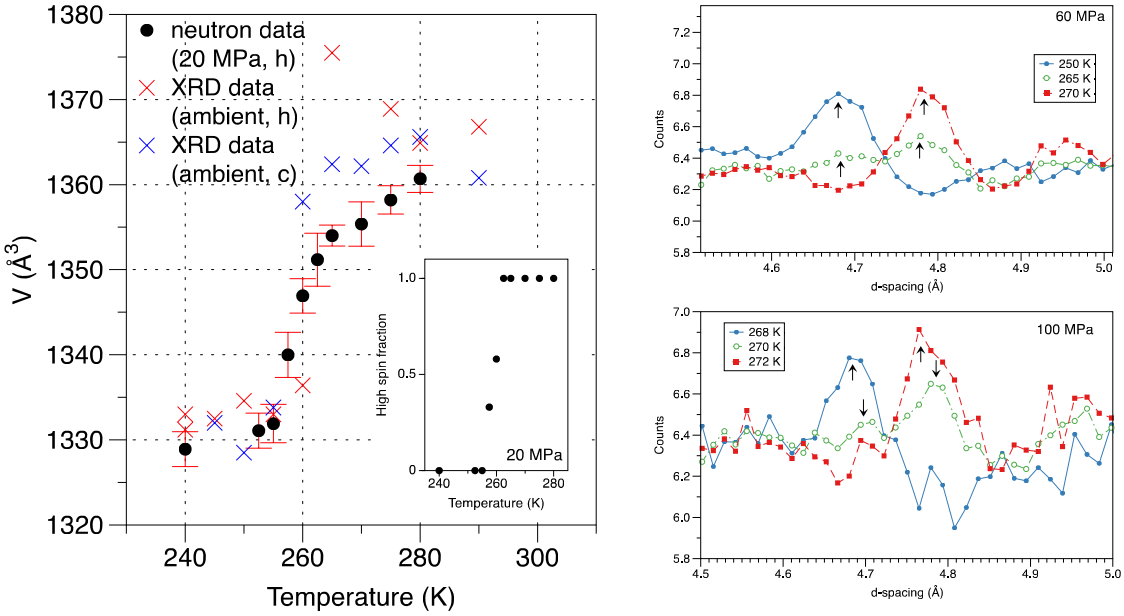

Figure 3. (Left) Results of Rietveld refinement of neutron diffraction data: volume vs temperature for protonated $[FeL_2][BF_4]_2$ in 20 MPa, obtained on heating. X-ray data (Table S2) are included for comparison with data taken on heating and cooling shown in red and blue, respectively. The esd errors in the x-ray refinements are no larger than the symbols used. The inset shows the fraction of high spin phase obtained from the refinement of neutron diffraction data in 20 MPa. (Right) Examples of raw data showing evidence of the SCO transition in 60 MPa (on heating) and 100 MPa (on cooling). Bragg peaks are indicated by arrows. Coexistence of HS and LS phases during the spin crossover is clearly visible in each case.

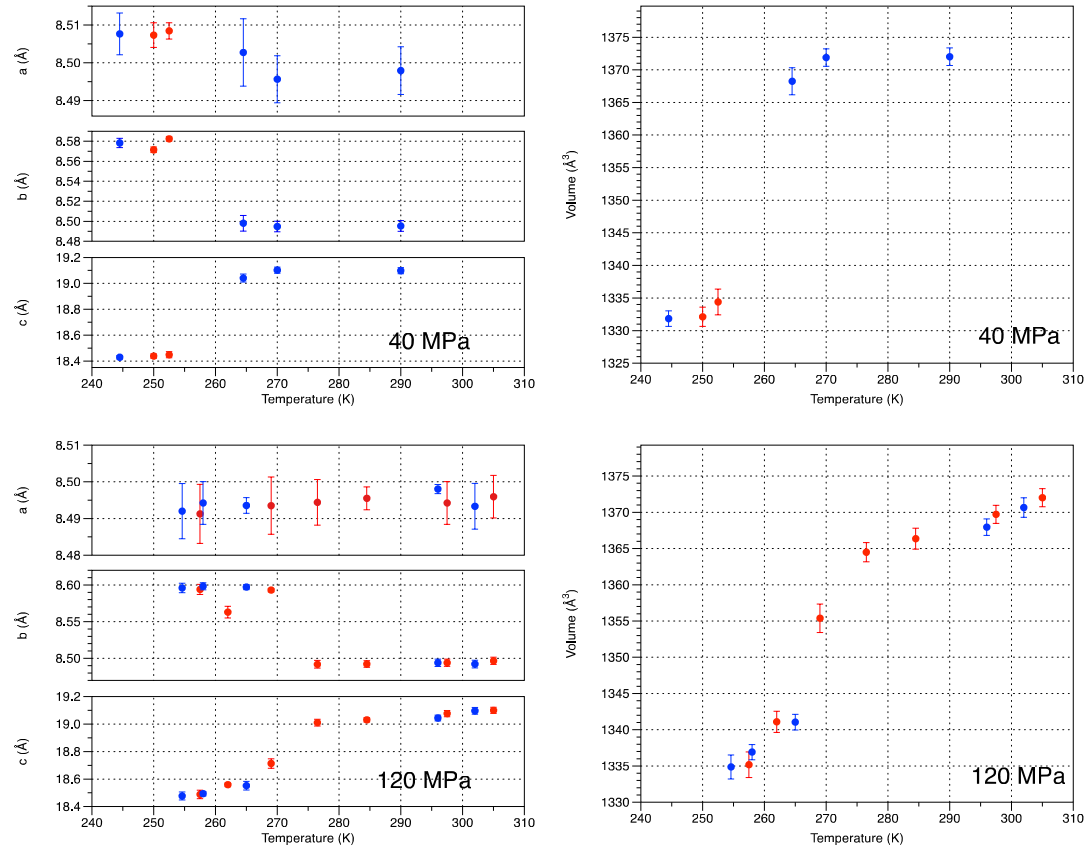

Figure 4. Results of Rietveld refinement of neutron diffraction data: temperature variation of the lattice parameters of partially deuterated $[FeL_2][BF_4]_2$ in 40 MPa (400 bar) and 120 MPa (1200 bar). Data taken on heating and cooling are shown in red and blue, respectively.

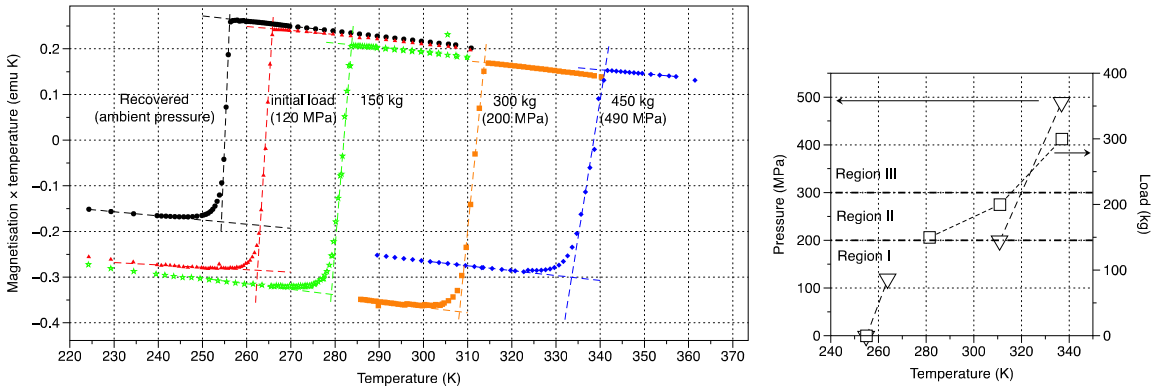

Figure 5. (Left) SQUID magnetometry for protonated $[FeL_2][BF_4]_2$ at pressures up to 490 MPa. Load levels in kilograms correspond to applied pressures of 120 MPa (initial load), 200 MPa (300 kgs) and 490 MPa (450 kgs) respectively. The pressure value for one curve (200 kgs of load) could not be uniquely assigned but is assumed to lie between 120 MPa and 200 MPa. We note that the ambient "recovered" pressure curve was taken last and that an irrecoverable phase transition has taken place in part of the sample at 490 MPa, as shown by the decreased drop in magnetization at the SCO transition. (Right) The (pressure,temperature) phase line shown in terms of applied pressure (left axis) or applied load (right axis). Approximate regions of low, medium and high pressure, as identified by the rate of change of spin crossover temperature, are denoted as regions I, II and III respectively.

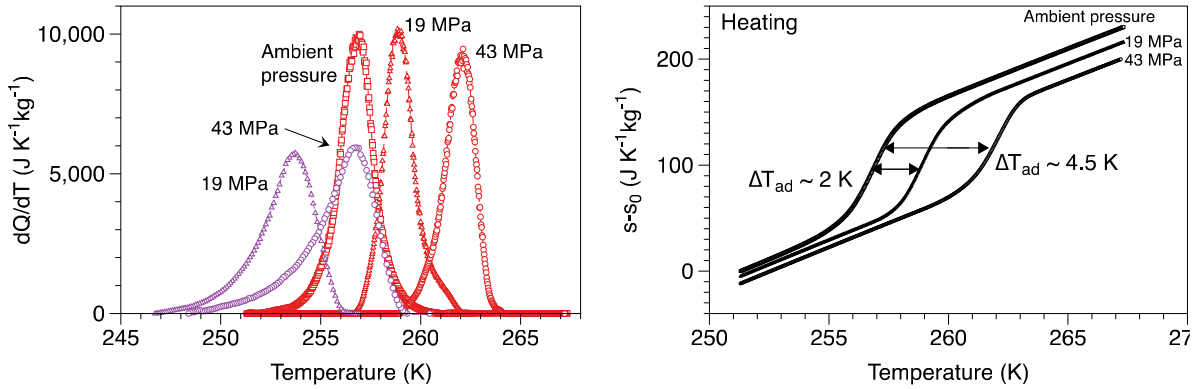

Figure 6. Calorimetry data on partially deuterated $[FeL_2][BF_4]_2$, showing how the spin crossover transition shifts in 19 MPa and 43 MPa on heating (red) and cooling (blue). Data in ambient conditions are shown in heating, only. Calculated entropy vs temperature showing that the maximum irreversible adiabatic temperature change in 19 MPa is 2 K and in 43 MPa is about 4.5 K. Entropy is plotted as s-s_0, where s_0 is the entropy at ambient pressure and 251 K, away from the phase transition. In the construction of the entropy curves, a fixed background heat capacity of $3R$ per mole-atom has been added. Reversible adiabatic temperature change effects are discussed in the text.